ACES

DOI: 10.1002/asia.201500690

CHEMISTRY
AN ASIAN JOURNAL
Full Paper

Chemosensors

Reversible and Selective Fluorescence Detection of Histidine Using a Naphthalimide-Based Chemosensing Ensemble

Qingtao Meng,*[a] Hongmin Jia,[a] Xue Gao,[a] Yue Wang,[a] Run Zhang,*[b] Renjie Wang,[c] and Zhiqiang Zhang[a]

Abstract: We described a new ensemble-approach-based chemosensor, NCH-Cu^{2+}, for highly selective and reversible detection of histidine (His) in aqueous solution and live cells. The ligand NCH exhibited specific binding with Cu^{2+} ions over other metal ions, accompanied with a 92.2% fluorescence quenching. The decomplexation of NCH-Cu^{2+} ensemble by His led to the liberation of the fluorophore, NCH, and thus the fluorescence was recovered. The specific fluorescence enhancement of NCH-Cu^{2+} towards His showed a good linearity with a detection of limit at 70 nM. Quantification of intracellular His at the single cell level was achieved by microscopy and flow cytometry. Besides the UV/Vis and emission titration, reversibility of the NCH-Cu^{2+} towards His was further confirmed by imaging and cytometry analysis. In addition, microscopy studies revealed that NCH-Cu^{2+} was distributed in the lysosome of live cells, where it could be employed as a fluorescent biosensor for imaging of His at subcellular level.

Introduction

Histidine (His), a building block of protein, is an essential bioactive amino acid in humans and other mammals.[1] It has been reported that His serves as a neurotransmitter or a neuromodulator in the mammalian central nervous system, and plays very crucial role in controlling metal transport in biologically important bases.[2] Recently, studies indicated that persistent deficiency of His may cause chronic kidney disease and pulmonary diseases.[3] On the other hand, overexpression of His in biological systems is associated with stress and psychological disorders.[2a] Therefore, rapid, selective quantification of His in aqueous solution, especially in biological samples, is of great importance.

In the past few years, considerable efforts have been devoted to the development of methods for the detection of His, including liquid chromatography,[4] capillary electrophoresis,[5] electrochemistry,[6] UV/Vis[7] or fluorescence spectroscopy.[8] Among these methods, spectrometric analysis using biosensors has been recognized as one of the most useful analytical technologies due to the high sensitivity and specificity, easy availability of instruments, capability of results interpretation even by naked eyes, and the potential for commercialization.[9] Thereby, quite a few biosensors have been developed in recent years,[10] including specific reaction-based chemodosimeters,[8e,11] ensemble-approach-based chemosensors,[12] and metal ions-modulated nanosensors.[8c,13] Nevertheless, a biosensor which could be employed as an imaging probe for the specific and quantitative detection of intracellular His, especially at subcellular level, remains a challenge for researchers.

Recently, the ensemble approach has emerged as a new platform for chemosensing and fluorescent imaging because of its unusual properties.[14] This strategy relies on the use of a dye bound to a receptor via a noncovalent interaction to form a new complex, ensemble. The replacement of the receptor by the analyte gives major variations in the optical features. In our previous research, by exploitation of the paramagnetic fluorescence quenching ability of Cu^{2+}, we also developed a series of ensemble-approach-based fluorescent chemosensors for the detection of anions in aqueous solution and successfully demonstrated their application in biological and environmental samples.[15] In the present work, we shifted our interest to the development of a fluorescent chemosensor for the discrimination of His from other amino acids in biological systems by using such a sensing-ensemble approach.

Therefore, a new Cu^{2+} ensemble, NCH-Cu^{2+}, has been designed and facilely synthesized for the quantitative detection of His in living cells with high specificity in this work

[a] Dr. Q. Meng, H. Jia, X. Gao, Y. Wang, Prof. Z. Zhang
Key Laboratory for Functional Material
Educational Department of Liaoning Province
University of Science and Technology Liaoning
Anshan 114051 (P.R. China)
E-mail: qtmeng@ustl.edu.cn

[b] Dr. R. Zhang
Department of Chemistry and Biomolecular Sciences
Faculty of Science and Engineering
Macquarie University
Sydney NSW, 2109 (Australia)
E-mail: run.zhang@mq.edu.au

[c] Dr. R. Wang
School of Chemistry and Molecular Biosciences
The University of Queensland
Brisbane, Queensland (Australia)

Supporting information for this article is available on the WWW under http://dx.doi.org/10.1002/asia.201500690.

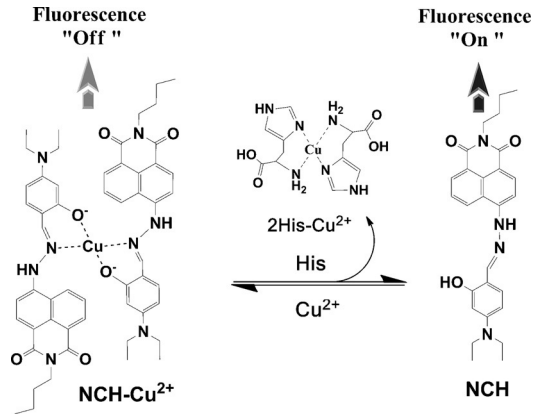

Scheme 1. Schematic illustration of the His chemosensor based on the NCH-Cu^{2+} ensemble.

(Scheme 1). The unique ligand, 1, 8-naphthalimide-based NCH[16] was employed for specific capture of Cu^{2+} ions to form a non-fluorescent complex ($K_a = 3.12 \times 10^6\ M^{-1}$), NCH-$Cu^{2+}$ ensemble. Subsequent effective snatching of Cu^{2+} ions from the NCH-Cu^{2+} ensemble in aqueous solution or biological samples by a Cu^{2+}-His binding can switch ON the fluorescence of the sensing ensemble via liberation of fluorophore, NCH. NCH has low cytotoxicity, and can enter the live cells through a temperature-dependent pathway. Confocal microscopy imaging in live U-343 MGa and MDA-MB-231 cells revealed that NCH is distributed in the lysosome after intracellular uptake. In addition, quantitative fluorescence detection of His was achieved by confocal microscopy and flow cytometry analysis.

Results and Discussion

Spectroscopic studies of NCH in the presence of Cu^{2+}

Firstly, the interaction of NCH with Cu^{2+} was investigated by UV/Vis spectrophotometric titration in HEPES buffer (THF: $H_2O = 3:7$, 20 mM, pH 7.4). As shown in Figure 1 A, NCH displays a major absorption band with a maximum absorption peak at about 510 nm in HEPES buffer. Upon an increase in the concentration of Cu^{2+} (0–2 equiv), a decrease in the absorbance peak at 510 nm with a hypochromatic shift of about 65 nm was observed, implicating the formation of a NCH-Cu^{2+} ensemble. In addition, the Cu^{2+} titration solution of NCH exhibited an obvious visible color change from pink to yellow (Figure 1 A) insert), indicating that NCH can serve as a "naked-eye" Cu^{2+} ions indicator in aqueous medium. The selective binding of NCH to Cu^{2+} was then examined by UV/Vis absorption spectrum (Figure S4 and S5, Supporting Information). Negligible changes of UV/Vis absorption spectrum and color were observed upon the addition of other competitive metal ions, including Ag^+, Co^{2+}, Ni^{2+}, Cd^{2+}, Zn^{2+}, Fe^{2+}, Cr^{3+}, Al^{3+}, Li^+, Ca^{2+}, Mg^{2+}, Ba^{2+}, K^+, Na^+, and Li^+.

To get further insight into the binding of Cu^{2+} with NCH, the fluorescence spectra of NCH with different equivalents of Cu^{2+} were recorded (Figure 1 B). NCH displayed strong fluorescence emission maximum at 523 nm in HEPES buffer ($\varphi_1 = 0.575$). Upon increasing the concentration of Cu^{2+} ions (0–20 μM), NCH exhibited significant quenching in the fluorescence intensity ($\varphi_2 = 0.075$) with a 12 nm bathochromic shift of the maximum emission. Job's plot evaluated from the fluorescence intensities of the titration solution showed the maximum at 0.33 (Figure S6, Supporting Information), which indicated that the NCH-Cu^{2+} binding has a 2:1 stoichiometry. Based on the 2:1 binding mode, the association constant (K_a) was evaluated using the Benesi–Hildebrand method and was found to be $3.12 \times 10^6\ M^{-1}$ (Figure S7, Supporting Information). Furthermore, the fluorescence changes of NCH at 523 nm exhibited a linear correlation to Cu^{2+} ions in the concentration range from 0 to 12 μM ($R^2 = 0.995$) (Figure S8, Supporting Information). The detection limit for Cu^{2+} ions was estimated to be 10 nM based on a 3ρ/slope.[15d] Fluorescence emission intensity changes upon addition of equal amounts of various cations including Ni^{2+}, Pb^{2+}, Zn^{2+}, Fe^{2+}, Fe^{3+}, Ag^+, Cd^{2+}, Co^{2+}, Cr^{3+}, Cu^{2+}, Al^{3+}, Mg^{2+}, Ca^{2+}, Ba^{2+}, K^+, Li^+, and Na^+ as nitrate salts in HEPES buffered at pH 7.4 were then studied. As shown in Figure S9, in the presence of 2.0 equiv of Cu^{2+} ions, the fluorescence of NCH (10 μM) was almost completely quenched (quenching efficiency at 523 nm, $(F_0-F)/F_0 \times 100\% = 92.2\%$), which could be ascribed to a paramagnetic quenching effect of Cu^{2+} ions.[15b,c,d] Nevertheless, no obvious changes of fluorescence intensity was observed in the presence of Ni^{2+}, Pb^{2+}, Zn^{2+}, Ag^+, Cd^{2+}, Co^{2+}, Cr^{3+}, Al^{3+}, Mg^{2+}, Ca^{2+}, Ba^{2+}, K^+, Li^+, and Na^+ at the same conditions. In addition, further addition of 20 μM Cu^{2+} ions to the above solution gave rise to a significant fluorescence quenching in accordance with the addition of equal amount of Cu^{2+} ions alone, indicating that Cu^{2+}-specific response was not disturbed by the competitive cations.

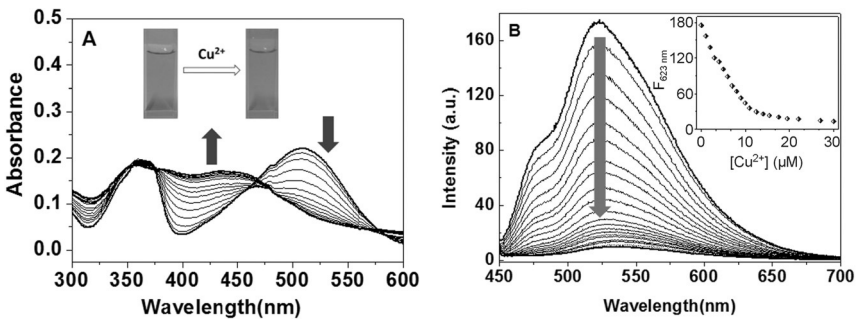

Figure 1. (A) Changes in the UV/Vis absorption spectra of NCH (10 μM) in HEPES buffer (THF:$H_2O = 3:7$, 20 mM, pH 7.4) with various amounts of Cu^{2+} ions (0–20 μM). Inset: the color change of NCH upon added of 20 μM Cu^{2+}; (B) fluorescence changes of NCH (10 μM) in HEPES aqueous buffer with different amounts of Cu^{2+} ions (0–30 μM). The inset exhibits a fluorescence titration profile at 523 nm upon the addition of Cu^{2+} ions, excitation at 430 nm.

Fluorescence response of NCH-Cu^{2+} towards His

The UV/Vis absorption response of NCH-Cu^{2+} ensemble towards His was then investigated by titration analysis. As shown in Figure 2A, the absorption band at 510 nm increased gradually after the addition of 30 μM His to the NCH-Cu^{2+} ensemble solution. The final absorption spectrum of the titration is as same as that of chemosensor NCH at the identical condition. Moreover, the color of NCH-Cu^{2+} ensemble solution recovered to pink from yellow upon the addition of His (Figure 2A, insert), suggesting that NCH-Cu^{2+} ensemble can serve as a "naked-eye" His visual indicator in aqueous media. In addition, the results on the UV/Vis spectra of NCH-Cu^{2+} ensemble with other important competitive species showed no obvious response, demonstrating that NCH-Cu^{2+} ensemble is selective towards His (Figure S10, Supporting Information).

Fluorescent response titration analysis was further examined in HEPES buffer to demonstrate the capability of NCH-Cu^{2+} ensemble as a chemosensor for His in detail. As shown in Figure 2B, upon the addition of increasing concentrations of His, the fluorescence was gradually recovered and the emission intensity of NCH-Cu^{2+} ensemble at 523 nm remained constant when up to 30 μM His was added (Figure S11, Supporting Information). The intensity and overall pattern of the emission spectrum closely match those of native NCH state ($\varphi_3 = 0.527$), indicating the liberation of ligand, NCH in the presence of His. The fluorescence increase showed a good linearity with the concentrations of His in the range of 0–5 μM. The detection limit was estimated to be 70 nM based on a 3ρ/slope by reported method (Figure S12, Supporting Information).[15d]

Next, the selectivity of NCH-Cu^{2+} ensemble towards His was evaluated in HEPES buffer by the examination of fluorescence intensities of NCH-Cu^{2+} ensemble with His and other physiological important amino acids, Hcys, GSH, and anions, including Ile, Ala, Arg, Asp, Cys, Glu, Gly, Hcys, Lue, Lys, Met, Phe, Pro, Ser, Thr, Try, Val, Asn, Gln, ADP, AMP, ATP, Cl^-, HCO_3^-, HSO_4^-, NO_2^-, NO_3^-, Pi, S^{2-}, and His. As shown in Figure 2C, significant fluorescence enhancement was observed only when the NCH-Cu^{2+} ensemble was treated with His. In addition, all of the potentially competitive amino acids, thiols and anions exhibited no obvious effect on the fluorescence response of NCH-Cu^{2+} ensemble towards His. The results demonstrated that NCH-Cu^{2+} is a His-specific fluorescence chemosensor even in complicated samples.

ESI-MS study was conducted to further investigate the proposed displacement mechanism of NCH-Cu^{2+} towards His. As shown in Figure S13, upon the addition of 2.0 equiv of Cu^{2+} ions into the HEPES buffer of NCH, the peaks at $m/z = 978.2$ and 1010.5 were found, which can be attributed to $[NCH\text{-}Cu + H]^+$ and $[NCH\text{-}Cu + CH_3OH + H]^+$, respectively. This result revealed that 2:1 stoichiometry complex between NCH and Cu^{2+} ions. Upon addition of His, ESI-MS displayed the peaks at $m/z =$ 976.2, which could be assigned to $[NCH\text{-}Cu\text{-}H]^-$. While, the peaks at $m/z = 457.1$, 479.2 can be attributed to $[NCH-H]^-$, and $[NCH + Na - 2H]^-$, and the peaks at $m/z = 372.0$, 410.1, 432.2 to be assigned to His-Cu products (Figure S14, Supporting Information). Therefore, the results indicated that the binding of His and Cu^{2+} led to the liberation of fluorophore, NCH.

The proposed chemosensor, NCH-based ensemble, NCH-Cu^{2+} was considered to be a reversible fluorescence chemosensor towards His in aqueous solution. As shown in Figure 2D, with alternate addition of Cu^{2+} and His, "ON-OFF-ON" changes in fluorescence intensity were observed, and these changes could be repeated more than 5 times, indicating that NCH can be developed as a reversible and renewable fluorescence chemosensor for His detection. Moreover, the effects of pH on the fluorescence

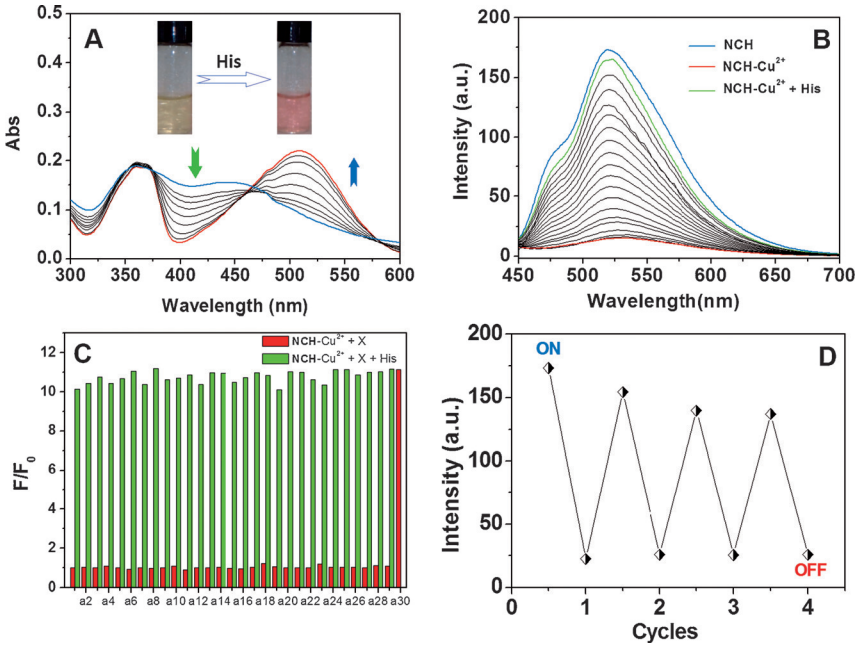

Figure 2. Changes in the UV/Vis absorption spectra (A) and emission spectra (B) of NCH-Cu^{2+} (10 μM) in the presence of various amounts of His (0–30 μM) in HEPES buffer; (C) normalized fluorescence responses of NCH-Cu^{2+} (10 μM) to various amino acids, bioactive anions, and thiols in HEPES buffer. The red bars represent the changes of fluorescent intensities of NCH-Cu^{2+} in the presence of competitive species of interest (all are 30 μM). The green bars represent the changes of the intensities that occur upon the subsequent addition of 30 μM of His to the above solution. a1 = Ile; a2 = Ala; a3 = Arg; a4 = Asp; a5 = Cys; a6 = Glu; a7 = Gly; a8 = Hcys; a9 = Lue; a10 = Lys; a11 = Met; a12 = Phe; a13 = Pro; a14 = Ser; a15 = Thr; a16 = Try; a17 = Val; a18 = Asn; a19 = Gln; a20 = ADP; a21 = AMP; a22 = ATP; a23 = Cl^-; a24 = HCO_3^-; a25 = HSO_4^-; a26 = NO_2^-; a27 = NO_3^-; a28 = Pi; a29 = S^{2-}; a30 = His. (D) Fluorescence intensity of NCH (10 μM) in HEPES buffer upon the alternate addition of Cu^{2+}/His to several concentration ratios (0:0, 20:0, 20:30, 40:30, 40:60, 70:60, 70:120, 130:120 μM, respectively). The intensities were recorded at 523 nm, excitation at 430 nm.

intensities of NCH and NCH-Cu^{2+} was evaluated in HEPES buffer with different pH from 4.5–11.0 (Figure S15, Supporting Information). The results suggested that the NCH-Cu^{2+} ensemble can be employed as a fluorescent chemosensor for His detection in weakly acidic, neutral, and basic buffer.

Fluorescence detection of His in live cells

Prior to the confocal microscopy imaging and flow cytometry analysis, the long-term cellular toxicity of NCH was evaluated by a MTT assay in human neuronal glioblastoma (U-343 MGa) and breast carcinoma (MDA-MB-231) cell lines 24 h post incubation.[17] As shown in Figure 3, upon incubation with different

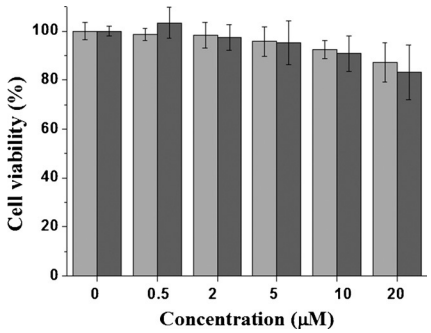

Figure 3. MDA-MB-231 (light grey) and U-343 MGa (grey) cell viability values (%) assessed using an MTT proliferation test versus incubation concentrations of NCH.

concentration of NCH (0, 0.5, 2, 5, 10, and 20 μM), U-343 MGa cell viabilities remained approximately 87%, and MDA-MB-231 cell viabilities remained more than 83% even with an incubation time of 24 h at the high concentration of 20 μM. The results demonstrated that NCH has low cytotoxicity both at low and high concentration and will not kill the U-343 MGa and MDA-MB-231 cells being probed.

Having demonstrated the high biocompatibility of NCH, we then evaluated its capability of cellular uptake in live U-343 MGa and MDA-MB-231 cells. The amphiphilicity of the proposed fluorescence imaging probe, NCH, was examined by measuring the partition coefficient ($\log P_{o/w}$) between 1-octanol and water.[18] The result showed that the $\log P_{o/w}$ of NCH was 0.67, indicating NCH could be a cell membrane permeable probe.

To further understanding the cellular entry pathway of NCH, subsequent investigation in detail was conducted under conditions of different temperatures and in the presence of metabolic and endocytic inhibitors.[10e,18b] First, the uptake of NCH was examined when the active transport pathway was blocked by incubation at 4 °C. As determined by the confocal microscopy analysis (Figure S16A, S17A, Supporting Information), the intracellular fluorescence intensity was significantly suppressed when the live U-343 MGa and MDA-MB-231 cells were incubated with 2 μM NCH at 4 °C.[19] Considering the fact that cell metabolism and physiological activities would be suppressed under low-temperature condition, we reasoned that energy-dependent pathways could be involved in the cellular uptake of NCH. It is well-known that endocytosis is a common energy-dependent uptake route that can be hampered under low temperature. Therefore, we then examined the effect of endocytic inhibitors, NH_4Cl and chloroquine, on the cellular uptake of NCH. As can be seen from the microscopy imaging analysis (Figure S16B, C; S17B, C, Supporting Information), relative strong intracellular fluorescence was observed in both U-343 MGa and MDA-MB-231 cells. Additionally, long incubation times are required for the endocytotic pathway. Thus, the results indicated that endocytotic pathway is not responsible for the cellular uptake of NCH.

Then, the reversible fluorescence response of NCH-Cu^{2+} towards His was evaluated in U-343 MGa and MDA-MB-231 cells by confocal microscopic and flow cytometric analysis. U-343 MGa and MDA-MB-231 cells were incubated with NCH for 30 min at 37 °C in a humidified, 5% CO_2/95% air (v/v) incubator, and then were sequentially treated with Cu^{2+} and His. As shown in Figure 4A, strong green fluorescence was observed when the U-343 MGa cells were incubated with 2 μM NCH for 30 min. When the NCH-loaded cells were treated with 10 μM Cu^{2+} for 30 min, the intracellular fluorescence become dim (Figure 4B), implying that the non-fluorescent NCH-Cu^{2+} ensemble was generated in U-343 MGa cells through complexation of Cu^{2+} ions with NCH. Further incubation of the cells with 100 μM His recovers the fluorescence signal, which suggest the decomplexation of NCH-Cu^{2+} by the addition of His (Figure 4C). Then, the reversibility of NCH towards His was further examined in U-343 MGa cells by the sequential treatment with Cu^{2+} and His. The fluorescence was quenched when the cells were treated with Cu^{2+}, and significantly enhanced when the cells were further incubated with His again (Figure 4D, E). The reversible fluorescence response towards His was further confirmed by confocal microscopy imaging in live MDA-MB-231 cells by sequential incubation with Cu^{2+} and His (Figure S18, Supporting Information). By the complexation/decomplexation interaction modulated by Cu^{2+}-His, the intracellular His level could be visualized by using NCH-Cu^{2+} as a chemosensor.

The changes of intracellular fluorescence intensities were further quantified by the flow cytometry assay by measuring the fluorescence of 10000 cells from each population. The shifts of histogram and the mean fluorescent intensity were recorded when the U-343 MGa and MDA-MB-231 cells were sequentially treated with Cu^{2+} and His. As shown in the bottom of Figure 4, S17, both U-343 MGa and MDA-MB-231 cells incubated only with NCH for 30 min showed a significant fluorescence from the histogram. Further incubation with Cu^{2+} shifts the histogram in the direction of non-fluorescent. However, the histogram shifts to the direction of strong fluorescence in the presence of His. Quantitative fluorescence intensity assay was achieved by the measurement of mean fluorescence intensity (Figure 5). The results demonstrated that reversible fluorescence response of NCH towards His could be achieved at single intact cell level.

We noticed that the spherical vesicles with bright green fluorescence diffused in the cytoplasm. This observation en-

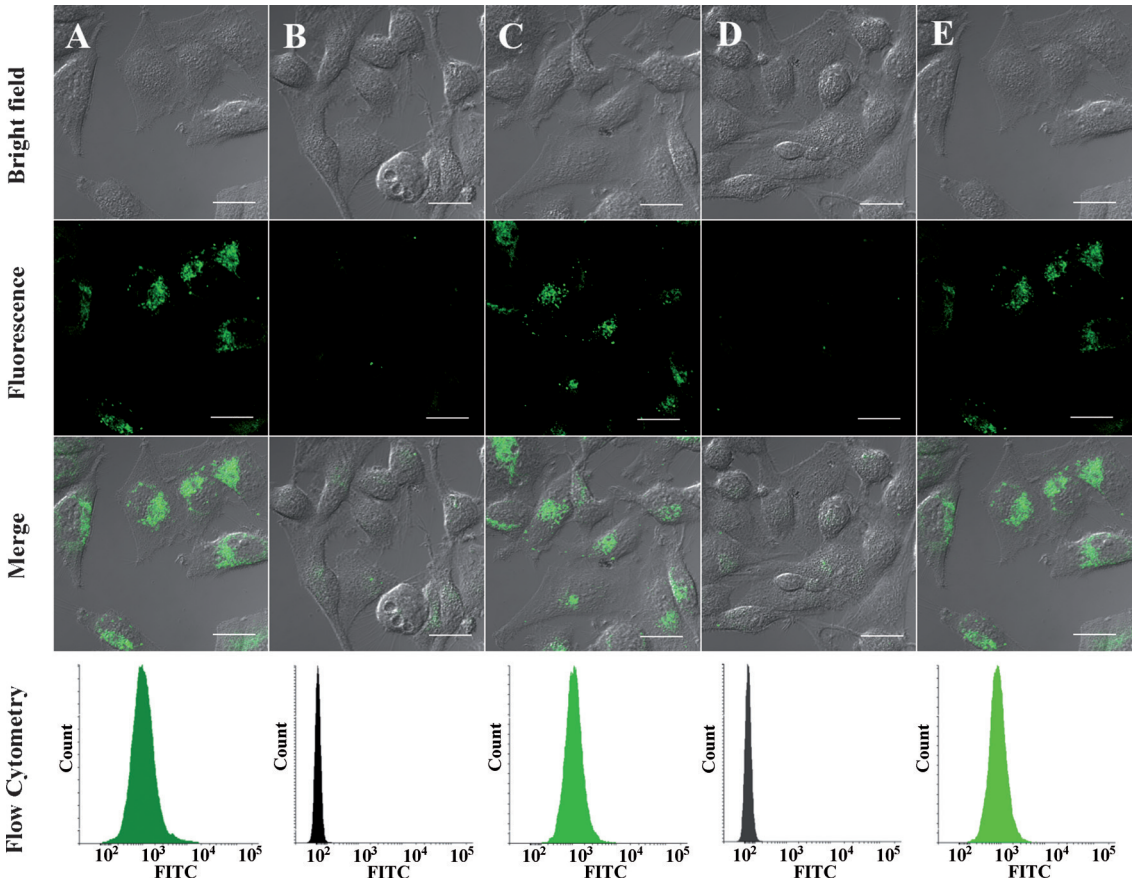

Figure 4. Confocal microscopy and flow cytometry analysis of reversible fluorescence response of NCH in live U-343 MGa cells. U-343 MGa cells were incubated with 2 μM NCH for 30 min, and then sequentially treated with Cu^{2+} (10 μM) and His (100 μM) for 30 min. The shifts of histograms of flow cytometric analysis represent the intracellular fluorescence intensity changes after U-343 MGa cells were treated with Cu^{2+} and His. Scale bar, 20 μm.

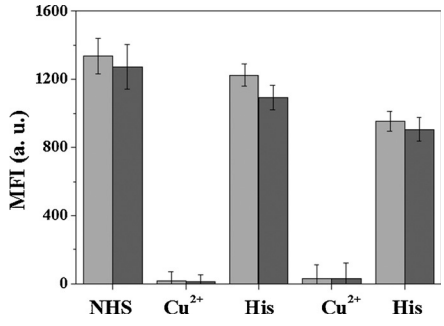

Figure 5. Mean fluorescence intensity per U-343 MGa (grey) and MDA-MB-231 (light grey) cell of different incubation conditions were examined by flow cytometric analysis.

couraged us to believe that NCH has organelle specificity probably lysosome, and could be potentially explored in targeted bioimaging studies. Thus, the colocalization assay was conducted in both live U-343 MGa and MDA-MB-231 cells by co-staining cells with NCH and commercial LysoTracker Red DND-99. As shown in Figure 6, S19, obvious overlap between the green fluorescence of NCH and the red luminescence of LysoTracker Red DND-99 was observed in both cell lines. The intensity profiles of the linear regions of interest across U-343 MGa and MDA-MB-231 cells stained with NCH and LysoTracker Red DND-99 also vary in close synchrony (Figure 6E, S19E, Supporting Information). The Pearson's correlation coefficients are 0.733 for U-343 MGa cells, 0.725 for MDA-MB-231 cells, and the Mander's overlap coefficients are 0.844 for U-343 MGa cells, 0.835 for MDA-MB-231 cells. All of the coefficients are close to 1, which represents high colocalization of NCH and LysoTracker Red DND-99 in both U-343 MGa and MDA-MB-231cells. In addition, a high correlation was found in the intensity scatter plot of Ch1 and Ch2 (Figure 6F, S19F, Supporting Information), suggesting the accumulation in the lysosome of NCH. Selecting a rectangular area on the intensity scatter plot, the corresponding white pixels on stimulated images were obtained in accordance with the overlay image, which corroborated that NCH is lysosome localized.

Then, we examined the utility of NCH-Cu^{2+} ensemble for the detection of His in live MDA-MB-231 and U-343 MGa cells by microscopy imaging and flow cytometry analysis. MDA-MB-231 and U-343 MGa cells were pretreated with 100 μM His for 2 h, followed by the further incubation with 2 μM NCH for another 30 min. Cells without His treatment were employed as the control group. As shown in Figure 7 and Figure S20, re-

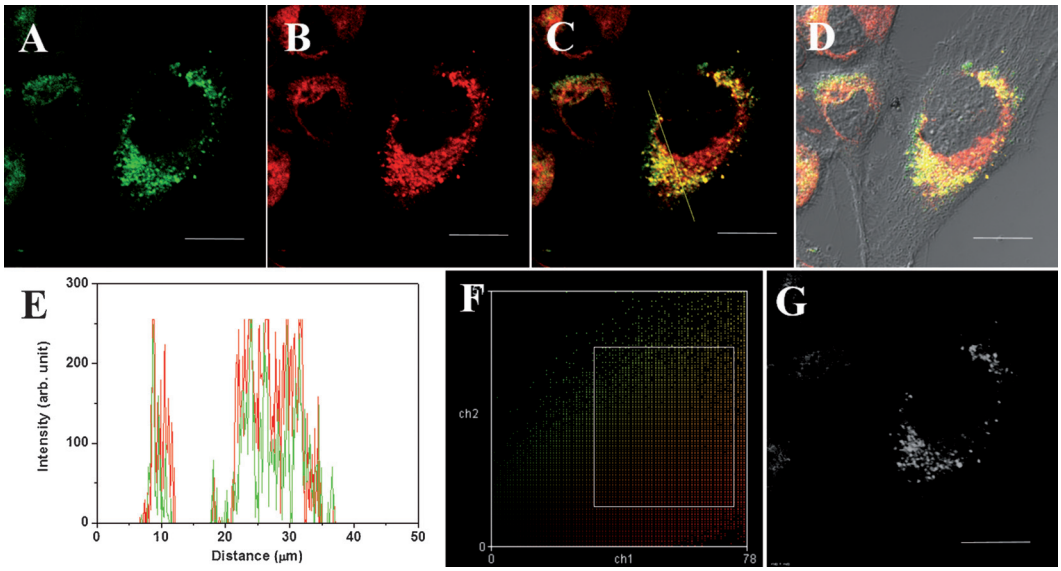

Figure 6. Confocal fluorescence colocalization imaging of intracellular distribution of NCH with LysoTracker Red DND-99 in live U-343 MGa cells. Images of U-343 MGa cells were incubated with NCH (A: channel 1, $\lambda_{ex}=473$ nm, $\lambda_{em}=490$–525 nm), and further stained with LysoTracker Red DND-99 (B: $\lambda_{ex}=559$ nm, $\lambda_{em}=560$–620 nm;). (C) Overlay of (A) and (B). (D) Merged images of C with its bright field. (E) Fluorescence intensity profiles of the linear region of interest across U-343 MGa cells in image C. (F) Intensity correlation plot of U-343 MGa cells that were colocalized with NCH and LysoTracker Red DND-99. (G) Simulated images (the white pixels represented by the intensity correlation plot (F) were highlighted by selecting the points with a white rectangular selection. Scale bar, 10 μm.

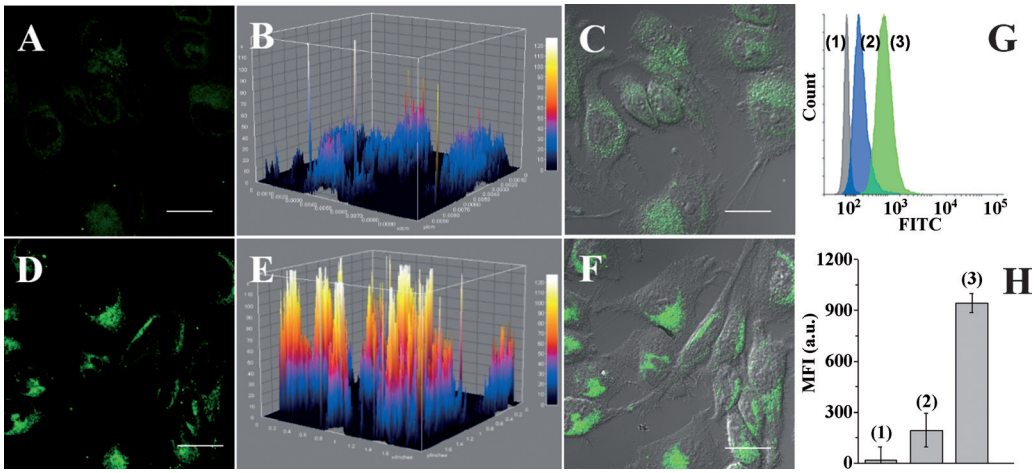

Figure 7. Confocal fluorescence imaging and flow cytometric assay of His in live U-343 MGa cells. (A, D) U-343 MGa cells were incubated with 2 μM NCH-Cu^{2+} for 30 min before (A) and after (D) treatment with 100 μM His for 2 h. (B, E) ImageJ 3D interactive intensity analysis of luminescence images of A and D; (C, F) merged images of A and D with their bright-field images. (G) Flow cytometry analysis results of live U-343 MGa cells (1, free cells; 2, NCH-Cu^{2+} loaded cells; 3, cells pre-treated with His and then stained with NCH-Cu^{2+}). (H) Mean luminescence intensity per U-343 MGa cell of (G1), (G2) and (G3) measured by flow cytometer. Scale bar, 20 μm.

markable fluorescence enhancement was observed from the fluorescence images and 3D interactive intensity analysis. And the increase of the fluorescence intensity was evaluated by the flow cytometry analysis by measuring the fluorescence intensities of 10000 cells. 4.8-fold, and 3.3-fold of fluorescence enhancement were obtained after the U-343 MGa and MDA-MB-231 cells were pretreated with 100 μM His (Figure 5G, H, S20G, H).

Conclusions

In summary, by exploration of the ensemble based strategy, a 1,8-naphthalimide-based fluorescent chemosensing ensemble, NCH-Cu^{2+}, has been developed for the highly selective and reversible detection of His in aqueous solution and living systems. The ensemble was derived from the complexation of NCH and Cu^{2+} ions, accompanied by a significant fluorescent quenching and an obvious shift of absorption wavelength which enables the detection to be performed by naked eyes.

In the presence of His, fluorescence and absorption recovery were observed due to the effective snatching of Cu^{2+} ions from NCH-Cu^{2+} ensemble. The detection limit of NCH-Cu^{2+} to His was estimated to be 70 nM. Low cytotoxicity of NCH was confirmed by the MTT analysis. Confocal microscopy imaging studies revealed that NCH could be transferred into the live MDA-MB-231 and U-343 MGa cells through an energy-dependent pathway. Sensitive, reversible and quantitative fluorescence detection of intracellular His was achieved by the confocal microscopy and flow cytometry analysis. Furthermore, co-localization analysis displayed that NCH is located in lysosomes after entering the live cells. We envisioned that such a NCH-Cu^{2+} ensemble could be further applied as a useful chemosensor for monitoring of His distribution in vivo.

Experimental Section

Synthesis of NCH

To a solution of 4-hydrazine-1, 8-naphthalimide (0.141 g, 0.5 mmol) in methanol (20 mL) was added 1.2 equiv of 4-diethyllaminosalicylaldhyde (0.116 g, 0.6 mmol), the reaction mixture was heated to reflux for 7 h. After cooling down to R. T., the red turbid solution was filtered and washed with methanol (5 mL) for three times to get NCH in 90% yield. Mp: 199.1–200.6 °C. ^{1}H NMR ([D$_6$]DMSO, 500 MHz): δ = 0.91 (t, 3H), 1.11 (m, 6H), 1.34 (m, 2H), 1.59 (m, 2H), 3.34 (m, 4H), 4.02 (m, 2H), 5.14 (s, 1H), 6.16 (s, 1H), 6.30 (t, J = 8.5 Hz, 1H), 7.43 (t, J = 4.0 Hz, 1H), 7.49 (t, J = 4.3 Hz, 1H), 7.74 (s, 1H),8.34 (d, J = 8.5 Hz, 1H), 8.46 (d, J = 7.0 Hz, 1H), 8.78 (d, J = 8.0 Hz, 1H), 10.21 (s, 1H), 11.22 ppm (s, 1H). ^{13}C NMR ([D$_6$]DMSO, 125 MHz): δ = 167.88, 163.78, 155.86, 155.42, 149.97, 149.37, 149.27. 135.05, 132.66, 132.03, 131.07, 129.00, 122.90, 121.82, 118.28, 110.53, 106.85, 106.70, 58.51, 49.36, 42.99, 29.86, 21.60, 18.35 ppm. IR: $\tilde{\nu}$ = 3737.55, 3419.51, 2965.70, 1583.55, 1387.04, 1519.53, 1287.36, 1121.63, 1237.86, 881.07, 773.08 cm^{-1}. API-ES spectra (negative mode, *m/z*): Calcd for $C_{27}H_{30}N_4O_3$: 458.2 [NCH]; Found: 457.2 [NCH < M- > H]$^-$). Elemental Analysis: Calculated: C, 70.72; H, 6.59; N, 12.22. Found: C, 70.63; H, 6.73; N, 12.25.

Confocal fluorescence imaging in living cells

Reversible imaging of His in living cells: MDA-MB-231, U-343 MGa cells were typically seeded at a density of 5×10^4 cells per mL in a 22 mm coverglass bottom culture dishes (ProSciTech, Australia) for the confocal microscope imaging. After 24 h, the culture media was replaced with fresh RPMI-1640 medium (MDA-MB-231, 2 mL per dish), or DMEM (U-343 MGa, 2 mL per dish) containing 2 μM NCH. The cells were incubated at 37 °C in a humidified, 5% CO_2/95% air (v/v) incubator for 30 min. After being washed with PBS (3×2 mL/dish), the NCH-loaded cells were then sequentially treated with Cu^{2+} (10 μM) and His (100 μM) for 30 min. The cells were washed with PBS (2 mL per dish) for three times before subjecting to confocal microscopy analysis.

Live cell imaging of NCH-Cu^{2+} towards His: MDA-MB-231, U-343 MGa cells were incubated with 100 μM His at 37 °C in a humidified, 5% CO_2/95% air (v/v) incubator for 2 h. After being washed with PBS (2 mL per dish) for three times, the cells were further stained with 2 μM NCH-Cu^{2+} for another 30 min. Then, the cells were subjected to confocal microscopy imaging after being washed with PBS (2 mL per dish) for three times.

Colocalization imaging of NCH in living cells: After being stained with 2 μM NCH for 30 min, washed with PBS (3×2 mL per dish), the MDA-MB-231, U-343 MGa cells were further incubated with 100 nM LysoTracker Red DND-99 for 30 min. Then, the confocal microscopy images were recorded after being washed with PBS (3× 2 mL/dish).

Cellular uptake of NCH. For examination of temperature-dependent cellular uptake of NCH, MDA-MB-231 and U-343 MGa cells were cooled at 4 °C for 30 min, then incubated with 2 μM NCH for 30 min under the same conditions. After being washed with PBS (3×2 mL per dish), the cells were subjected to the confocal microscopy imaging. For studying the effect of endocytotic inhibitors on cellular uptake of NCH, the cells were treated with NH_4Cl (10 mM), chloroquine (100 μM) for 30 min before the incubation with 2 μM NCH for 30 min at 37 °C in a humidified, 5% CO_2/95% air (v/v) incubator. Before imaging, the cells were washed with PBS (2 mL per dish) for three times.

Flow cytometry analysis

Reversible fluorescence response of His by the chemosensor NCH-Cu^{2+} was further assessed by means of flow cytometry analysis. MDA-MB-231 and U-343 MGa cells (1×10^5 cells per mL) were seeded into a six-chamber culture well and incubated for 24 h. For the analysis reversible fluorescence response of His in living cells, cells were incubated with 2 μM NCH for 30 min, washed with PBS for three times, and then sequentially treated with Cu^{2+} and His. For the analysis of intracellular His, the cells were treated with 100 μM His for 2 h before incubation with 2 μM NCH-Cu^{2+} for 30 min. Cells incubated with culture medium for 24 h were used as the controls for all experiments. All cells were detached from the well using 0.05% trypsin-EDTA solution and washed with PBS for three times before flow cytometry analysis.

Acknowledgements

We would like to acknowledge financial supports from the National Natural Science Foundation of China(No. 21301011), the Key Laboratory Program of Educational Department of Liaoning Province(LZ2015047), and Macquarie University Research Fellowship Scheme(MQRF-1487520). The authors also would like to thank Dr. Xiaoyi Xin at Dalian Institute of Chemical Physics, Chinese Academy of Sciences for NMR analysis.

Keywords: chemosensor · fluorescence imaging · histidine · lysosome · quantification

[1] J. Lemire, Y. Milandu, C. Auger, A. Bignucolo, V. P. Appanna, V. D. Appanna, *FEMS Microbiol. Lett.* **2010**, *309*, 170–177.
[2] a) M. Watanabe, M. E. Suliman, A. R. Qureshi, E. Garcia-Lopez, P. Bárány, O. Heimbürger, P. Stenvinkel, B. Lindholm, *Am. J. Clin. Nutr.* **2008**, *87*, 1860–1866; b) K. I. Varughese, *Histidine Kinases in Signal Transduction* (Eds.: M. Inouye, R. Dutta), Academic Press, San Diego, **2003**, 203.
[3] D. J. Sullivan, I. Y. Gluzman, D. E. Goldberg, *Science* **1996**, *271*, 219–222.
[4] N. Tateda, K. Matsuhisa, K. Hasebe, N. Kitajima, T. Miura, *J. Chromatogr. B* **1998**, *718*, 235–241.
[5] M. K. Amini, S. Shahrokhian, S. Tangestaninejad, *Anal. Chem.* **1999**, *71*, 2502–2505.
[6] a) Z. Huang, J. Du, J. Zhang, X.-Q. Yu, L. Pu, *Chem. Commun.* **2012**, *48*, 3412–3414; b) K. Kurzątkowska, D. Shpakovsky, J. Radecki, H. Radecka, Z. J. Wei, E. Milaeva, *Talanta* **2009**, *78*, 126–131.

[7] a) S.-K. Sun, K.-X. Tu, X.-P. Yan, *Analyst* **2012**, *137*, 2124 – 2128; b) S. Zhang, C. Yang, W. Zhu, B. Zeng, Y. Yang, Y. Xu, X. Qian, *Org. Biomol. Chem.* **2012**, *10*, 1653 – 1658.
[8] a) Y.-R. Liu, R. Hu, T. Liu, X.-B. Zhang, W. Tan, G.-L. Shen, R.-Q. Yu, *Talanta* **2013**, *107*, 402 – 407; b) P. Wu, X.-P. Yan, *Biosens. Bioelectron.* **2010**, *26*, 485 – 490; c) Y. He, X. Wang, J. Zhu, S. Zhong, G. Song, *Analyst* **2012**, *137*, 4005 – 4009; d) S. Qiu, M. Miao, T. Wang, Z. Lin, L. Guo, B. Qiu, G. Chen, *Biosens. Bioelectron.* **2013**, *42*, 332 – 336; e) D.-L. Ma, W.-L. Wong, W.-H. Chung, F.-Y. Chan, P.-K. So, T.-S. Lai, Z.-Y. Zhou, Y.-C. Leung, K.-Y. Wong, *Angew. Chem. Int. Ed.* **2008**, *47*, 3735 – 3739; *Angew. Chem.* **2008**, *120*, 3795 – 3799; f) J. Du, Z. Huang, X.-Q. Yu, L. Pu, *Chem. Commun.* **2013**, *49*, 5399 – 5401.
[9] a) X. Liu, Z. Ye, W. Wei, Y. Du, J. Yuan, D. Ma, *Chem. Commun.* **2011**, *47*, 8139 – 8141; b) Y. Xiao, R. Zhang, Z. Ye, Z. Dai, H. An, J. Yuan, *Anal. Chem.* **2012**, *84*, 10785 – 10792.
[10] a) R. Kumar Pathak, K. Tabbasum, V. Kumar Hinge, C. Pulla Rao, *Chem. Eur. J.* **2011**, *17*, 13999 – 14003; b) L. Fabbrizzi, G. Francese, M. Licchelli, A. Perotti, A. Taglietti, *Chem. Commun.* **1997**, 581 – 582; c) R. Yang, K. Wang, L. Long, D. Xiao, X. Yang, W. Tan, *Anal. Chem.* **2002**, *74*, 1088 – 1096; d) M. Kruppa, C. Mandl, S. Miltschitzky, B. König, *J. Am. Chem. Soc.* **2005**, *127*, 3362 – 3365; e) M. A. Hortalá, L. Fabbrizzi, N. Marcotte, F. Stomeo, A. Taglietti, *J. Am. Chem. Soc.* **2003**, *125*, 20 – 21; f) S.-h. Fujishima, H. Nonaka, S.-h. Uchinomiya, Y. A. Kawase, A. Ojida, I. Hamachi, *Chem. Commun.* **2012**, *48*, 594 – 596.
[11] a) C. Li, M. Yu, Y. Sun, Y. Wu, C. Huang, F. Li, *J. Am. Chem. Soc.* **2011**, *133*, 11231 – 11239; b) E. Oliveira, C. Santos, P. Poeta, J. L. Capelo, C. Lodeiro, *Analyst* **2013**, *138*, 3642 – 3645.
[12] a) H.-I. Un, S. Wu, C.-B. Huang, Z. Xu, L. Xu, *Chem. Commun.* **2015**, *51*, 3143 – 3146; b) T. Chen, L. Yin, C. Huang, Y. Qin, W. Zhu, Y. Xu, X. Qian, *Biosens. Bioelectron.* **2015**, *66*, 259 – 265; c) Q.-H. You, A. W.-M. Lee, W.-H. Chan, X.-M. Zhu, K. C.-F. Leung, *Chem. Commun.* **2014**, *50*, 6207 – 6210; d) J.-T. Hou, K. Li, K.-K. Yu, M.-Y. Wu, X.-Q. Yu, *Org. Biomol. Chem.* **2013**, *11*, 717 – 720; e) R. K. Pathak, J. Dessingou, C. P. Rao, *Anal. Chem.* **2012**, *84*, 8294 – 8300; f) G. Sivaraman, T. Anand, D. Chellappa, *ChemPlusChem* **2014**, *79*, 1761 – 1766.
[13] X. Zheng, T. Yao, Y. Zhu, S. Shi, *Biosens. Bioelectron.* **2015**, *66*, 103 – 108.
[14] a) J. Wu, B. Kwon, W. Liu, E. V. Anslyn, P. Wang, J. S. Kim, *Chem. Rev.* **2015**, *115*, 7893 – 7943; b) S.-R. Liu, C.-Y. Chang, S.-P. Wu, *Anal. Chim. Acta* **2014**, *849*, 64 – 69.
[15] a) Q. Meng, R. Zhang, H. Jia, X. Gao, C. Wang, Y. Shi, A. V. Everest-Dass, Z. Zhang, *Talanta* **2015**, *143*, 294 – 300; b) Q. Meng, Y. Wang, M. Yang, R. Zhang, R. Wang, Z. Zhang, *RSC Adv.* **2015**, *5*, 53189 – 53197; c) Q. Meng, Y. Shi, C. Wang, H. Jia, X. Gao, R. Zhang, Y. Wang, Z. Zhang, *Org. Biomol. Chem.* **2015**, *13*, 2918 – 2926; d) R. Zhang, X. Yu, Y. Yin, Z. Ye, G. Wang, J. Yuan, *Anal. Chim. Acta* **2011**, *691*, 83 – 88.
[16] a) H. Un, C.-B. Huang, C. Huang, T. Jia, X.-L. Zhao, C.-H. Wang, L. Xu, H.-B. Yang, *Org. Chem. Front.* **2014**, *1*, 1083 – 1090; b) H. Un, C.-B. Huang, J. Huang, C. Huang, T. Jia, L. Xu, *Chem. Asian J.* **2014**, *9*, 3397; c) L. Xu, Y. Xu, W. Zhu, C. Yang, L. Han, X. Qian, *Dalton Trans.* **2012**, *41*, 7212 – 7217.
[17] R. Zhang, B. Song, Z. Dai, Z. Ye, Y. Xiao, Y. Liu, J. Yuan, *Biosens. Bioelectron.* **2013**, *50*, 1 – 7.
[18] a) H. Komatsu, K. Yoshihara, H. Yamada, Y. Kimura, A. Son, S. Nishimoto, K. Tanabe, *Chem. Eur. J.* **2013**, *19*, 1971 – 1977; b) M. R. Gill, J. Garcia-Lara, S. J. Foster, C. Smythe, G. Battaglia, J. A. Thomas, *Nat. Chem.* **2009**, *1*, 662 – 667.
[19] H. Jia, X. Gao, Y. Shi, N. Sayyadi, Z. Zhang, Q. Zhao, Q. Meng, R. Zhang, *Spectrochim. Acta Part A* **2015**, *149*, 674.

Manuscript received: July 4, 2015
Accepted Article published: July 31, 2015
Final Article published: August 20, 2015